JTE HCMUTE
ISSN: 2615-9740

JOURNAL OF TECHNICAL EDUCATION SCIENCE
Ho Chi Minh City University of Technology and Education
Website: https://jte.edu.vn/
Email: jte@hcmute.edu.vn

Synchronous Sliding Mode Control for a 4-DOF Parallel Manipulator in Practice

Duc Thien Tran*, Thanh Nha Nguyen, Minh Tam Nguyen, Van Thuyen Ngo, Hoang Lam Le
Department of Automatic Control, Ho Chi Minh City University of Technology and Education, Vietnam

* Corresponding author. *Email: thientd@hcmute.edu.vn*

ARTICLE INFO

Received: 07/01/2023
Revised: 31/01/2023
Accepted: 16/02/2023
Published: 28/08/2023

KEYWORDS

Parallel robot;
Sliding mode control;
Synchronous control;
Cross-coupling error;
Lyapunov.

ABSTRACT

This paper proposes a synchronous sliding mode control (SSMC) method for a 4-DOF parallel robot model in practice with the influence of uncertain dynamics such as friction, external noise, and model error. A closed kinematic chain structure characterizes the parallel robot. The moving platform is controlled by four kinematic chains working together to follow a predetermined trajectory. However, traditional control methods only control each joint individually; if one of the actuators fails or has an external force, it can lead to system breakdown. Therefore, synchronous control to coordinate the operation of the arms is necessary. The synchronization algorithm is characterized by the cross-coupling error, which is the combination of tracking and synchronization errors for the system to achieve the synchronization goal. Cross-coupling error is used to design the sliding surface of the SSMC. The advantages of sliding mode control (SMC) are that it resists the influence of uncertain dynamics and it is combined with the synchronization algorithm. A control law is developed based on the sliding surface to ensure simultaneous convergence of both tracking and synchronization errors towards zero. The stability of the system is proven using the Lyapunov theory. In order to verify the effectiveness of the proposed approach, a 4-DOF parallel robot testbench is constructed. The SSMC controller results are compared with the testbench's proportional-integral-derivative (PID), synchronous proportional-integral-derivative (SPID), and SMC controllers.

Doi: https://doi.org/10.54644/jte.78A.2023.1322

1. Introduction

A parallel robot is made up of a moving platform attached to a fixed base by a set of identical parallel kinematic sequences. Each kinematic chain comprises two links, the upper and lower arm links, linked to each other and the moving platform by spherical joints. Therefore, it forms a closed-loop structure. Because of this special structure, the parallel robot has outstanding advantages over the open-loop serial robot, such as high rigidity, high operating speed, high accuracy, and large load-carrying capacity. However, there are some disadvantages of parallel robots such as the limitation of working space, the singularity configurations in the active space, and the complexity of the forward kinematics and dynamics of the robot [1], [2], leading to difficulties in controlling the robot. To address this issue, scientists have carried out many studies and published many works such as PI controller [3], Augmented Nonlinear PD controller [4], and nonlinear PID controller for a 6-DOF parallel robot [5]. Most of these controllers do not provide good performance control when the system is affected by external noise and the existence of uncertainty components such as friction and model error. So, advanced algorithms such as CTC [6]-[8] are applied to overcome the mentioned problems above. Nevertheless, the disadvantage of the CTC controller is that the accuracy of both dynamic and physical parameters related to the system is required for the controller to bring good performance. Meanwhile, due to the wear and tear of mechanical parts, and deviation of sensors during the operation of real systems, the requirement for the accuracy of the parameters is not feasible. Therefore, an SMC has been developed to manage the system changes and the variation of parameters and external noise [9]-[11] and has improved the system performance significantly. Nonetheless, the principle of parallel robot control is that the arms work together to move the moving platform to follow the preset trajectory. So, the synchronization among the

transmission joints should be considered, which the above controllers do not mention, and this problem has attracted many scientists and research organizations worldwide.

The synchronization algorithm was first introduced by Koren in 1980 [9]. The fundamental difference between synchronous and conventional controllers is the response to the synchronization error. Moreover, the cross-coupling error is a combination of tracking and synchronization errors to achieve the synchronization goal. It is also used to design synchronous controllers for closed-loop structure robots, such as the nonlinear PD synchronous controller for a 3-DOF parallel robot [10], synchronous sliding mode control for 2-DOF parallel structure [11], [12], and synchronous tracking control of a 6-DOF hydraulic parallel manipulator [13]. However, no individual or research organization has applied the synchronization algorithm to the 4-DOF parallel structure. Most studies are mainly done on simulations and a few experimental studies. Therefore, combining the synchronization algorithm with the SMC is necessary to design an SSMC for a 4-DOF parallel robot model.

From the analysis above, this paper proposes an SSMC for a 4-DOF parallel robot model in practice. Four AC servo motors are used in the test bench's construction, and they are set to torque control mode which drives four arms to work together to follow a predetermined trajectory. The synchronization algorithm is researched and developed, and the cross-coupling error is used to design the sliding surface of the SSMC. Therefore, the system performance is improved under the variation of uncertain parameters and external noise. At the same time, synchronization among the transmission joints of the system is also considered, so the end-effector of the robot achieves good tracking quality. The Lyapunov theory analyzes and establishes the stability of the system. Additionally, a practical 4-DOF parallel robot is constructed, and the proposed control is implemented on the test bench. Then, the results of the proposed approach are compared with the PID, SPID, and SMC controllers to prove the effectiveness of the proposed control.

The paper is organized into the following. Part 2 presents the structure of the test bench. Part 3 presents the solution to the inverse kinematics problem and discusses the problems in the forward kinematics and dynamics of the robot. Then, the control methods and proposal are presented in part 4. Part 5 provides the experimental results of the controllers and presents the error evaluation method of the controllers. Finally, part 6 presents the conclusions and future works.

2. Experimental setup

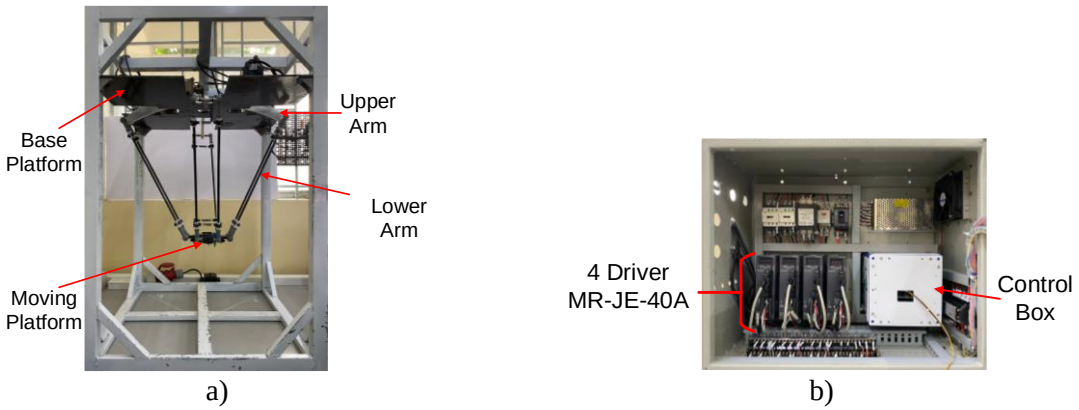

Figure 1. *A parallel 4-DOF robot test bench: (a) A parallel 4-DOF robot model; (b) A control cabinet*

The experimental test bench is constructed as depicted in Figure 1. Figure 1(a) presents a 4-DOF parallel robot model. The robot frame is made of iron. The four upper arms are made of aluminum and attached to four Mitsubishi AC Servo motors. The four lower arms are made of carbon, and the moving platform is made of plastic. Next, Figure 1(b) shows the robot control cabinet. It includes four drivers MR JE-40A controlling four AC servo motors. The MCU STM32F407VG does the calculation and provides an analog signal for drivers to control the motors. Finally, the experimental diagram of a 4-DOF parallel robot system is presented in Figure 2.

JTE
HCMUTE
ISSN: 2615-9740

JOURNAL OF TECHNICAL EDUCATION SCIENCE
Ho Chi Minh City University of Technology and Education
Website: https://jte.edu.vn/
Email: jte@hcmute.edu.vn

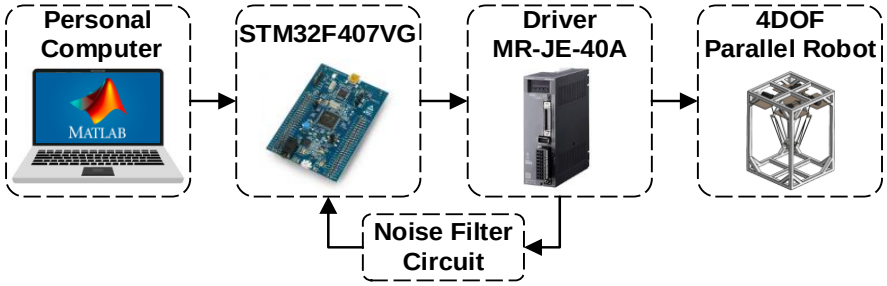

Figure 2. *Diagram of the experimental system*

3. Problem Formulations

3.1. Kinematics model

In this section, the inverse kinematics of the robot is presented, and some remaining issues in the forward kinematics are also discussed. The following notations are used in the formulations and are shown in Figure 3.

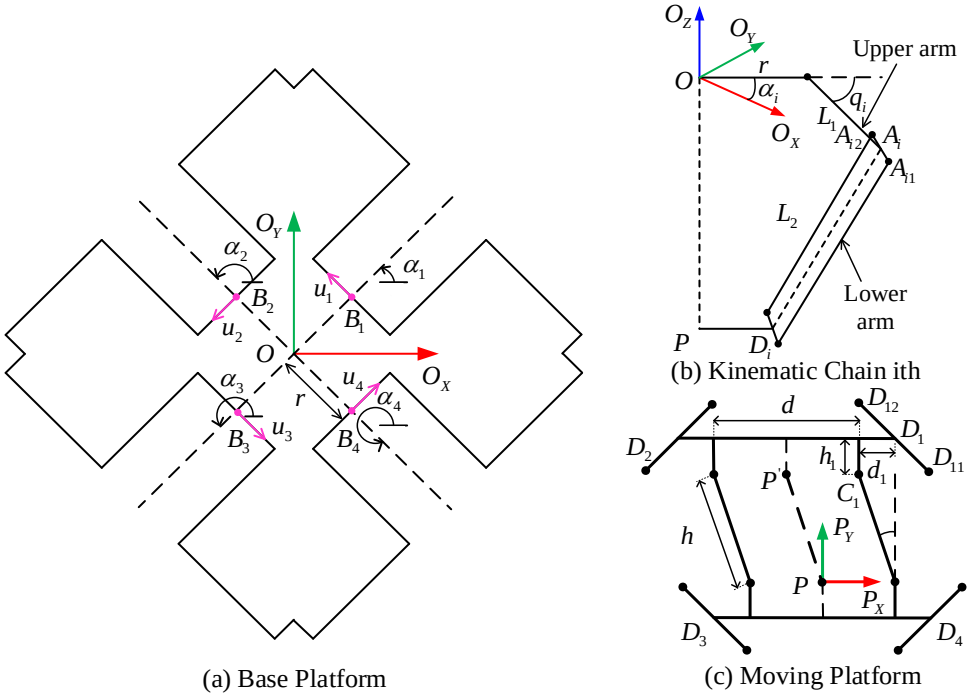

Figure 3. *Geometric structural overview of the robot*

where O_{XYZ} is the fixed base coordinate system; P_{XYZ} is the moving platform coordinate system; $\alpha_i \left(\alpha_1 = 45^\circ; \alpha_2 = 135^\circ, \alpha_3 = 225^\circ, \alpha_4 = 315^\circ\right)$ is the corresponding angles of each arm relative to the O_{XYZ} original coordinate system; B_i is the center of the actuated joint; u_i is the unit vectors along actuated joints; A_{i1} and A_{i2} are the centers of the spherical joints on the arm ith; $q_i \left(i = 1,2,3,4\right)$ is the actuated joint angles ith; L_1 is the upper arm length; L_2 is the lower arm length; D_{i1} and D_{i2} are the centers of the spherical joints on the moving platform; A_i is the middle of $[A_{i1}, A_{i2}]$; D_i is the middle of $[D_{i1}, D_{i2}]$; $\mathbf{a_i} = \overrightarrow{A_i D_i}$; h_i and d_i are distances between C_i and D_i, respectively, along P_Y axis and along P_X axis; d is the moving platform length; X, Y, Z is the position of the end-effector; θ is the rotation angle of the moving platform.

The parallel robot possesses the traits of a closed-loop construction, so it has the following kinematic constraint:

$$\left\|\overrightarrow{A_iD_i}\right\| = \mathbf{a_i}^2 = L_2^2 \left(i = 1,2,3,4\right) \quad (1)$$

The A_i can be inferred from the geometric function between q_i, α_i and L_1. For D_i, based on the physical parameters (d, h, d_1, h_1) and orientation θ of the moving platform, we can also write a geometric function representing the relationship between them.

Finally, equation (1) is a system of four equations that can be written as:

$$E_i \sin q_i + F_i \cos q_i + G_i = 0 \quad (2)$$

where E_i, F_i, G_i are based on the geometry of the robot.

By resolving each equation in the system (2), the IKP is solved. The following final solution is available based on the working area of the robot:

$$q_i = 2\tan^{-1}\left(\frac{-E_i - \sqrt{E_i^2 + F_i^2 + G_i^2}}{G_i - F_i}\right) \quad (3)$$

The solution of the FKP is to determine the position of the end effector in the workspace when joint angles q_i are known. However, as described in [2], this is not possible. But in this case, it is possible to use Newton Raphson method [14] to obtain an approximate solution of the absolute coordinate using the Jacobian matrix $\mathbf{J}$ and the relation of inverse kinematics.

$$\mathbf{P_{n+1}} = \mathbf{P_n} + \mathbf{J}(\mathbf{X_n}, \mathbf{q_n})\left[\mathbf{q_d} - \mathbf{q_n}\right] \quad (4)$$

where $\mathbf{P_n}$ is the actual position coordinate of the end effector; $\mathbf{P_{n+1}}$ is the next position coordinates of the end effector; $\mathbf{q_n}$ is the actual joint angle; $\mathbf{q_d}$ is the desired joint angle.

Assumption 1. Tolerances at the joints of the robot are negligible, so corresponding to each set value of the joint angle, the position of the end-effector approximately to set position value from the circle orbital equation at each time t.

3.2. Dynamics model

The dynamic model of a 4-DOF parallel robot is given as follows:

$$\mathbf{M}(\mathbf{q})\ddot{\mathbf{q}} + \mathbf{C}(\mathbf{q}, \dot{\mathbf{q}})\dot{\mathbf{q}} + \mathbf{G}(\mathbf{q}) + \boldsymbol{\tau}_\mathbf{f} = \boldsymbol{\tau} \quad (5)$$

where $\mathbf{M}(\mathbf{q}) \in \Re^{4\times4}$ is the inertial matrix, $\mathbf{C}(\mathbf{q}, \dot{\mathbf{q}}) \in \Re^{4\times4}$ is the Coriolis/Centrifugal matrix, $\mathbf{G}(\mathbf{q}) \in \Re^{4\times1}$ is the acceleration vector of gravity, $\boldsymbol{\tau}_\mathbf{f} \in \Re^{4\times1}$ is the friction vector, $\mathbf{q}, \dot{\mathbf{q}}, \ddot{\mathbf{q}} \in \Re^{4\times1}$ are the vectors of the position, velocity, and acceleration of the joint angles, $\boldsymbol{\tau} \in \Re^{4x1}$ is the vector of applied joint torques.

Because the dynamics of a 4-DOF parallel robot are very complex, eq (5) can be rewritten as:

$$\ddot{\mathbf{q}} + \mathbf{d(t)} = \boldsymbol{\tau} \quad (6)$$

where $\mathbf{d}(\mathrm{t}) = \left(\mathbf{M}(\mathbf{q}) - \mathbf{I}\right)\ddot{\mathbf{q}} + \mathbf{C}(\mathbf{q}, \dot{\mathbf{q}})\dot{\mathbf{q}} + \mathbf{G}(\mathbf{q}) + \boldsymbol{\tau}_\mathbf{f}$, $\mathbf{d}(\mathrm{t}) \in \Re^{4x1}$ is the total uncertainty of the system, $\mathbf{I} \in \Re^{4\times4}$ is the unit matrix.

3.3. Cross-coupling error and synchronization error definitions

The synchronization of the parallel robot system is considered through the synchronization algorithm. This algorithm consists of two components: synchronization error and cross-coupling error. The following defines the system synchronization error:

$$\boldsymbol{\varepsilon}_i(t) = \mathbf{e}_i(t) - \mathbf{e}_{i+1}(t) = \mathbf{He}(t), (i = 1,2,3,4) \quad (7)$$

where $\mathbf{e}_i(t) = \mathbf{q}_{d_i}(t) - \mathbf{q}_i(t)$ is the tracking error of the joint ith, $\mathbf{q}_{d_i}(t)$ is the desired signal of the joint ith, $\mathbf{q}_i(t)$ is the response signal of the joint ith. In order to achieve synchronization in the system, a boundary condition is when $i = 4, i+1 = 1$.

To make both tracking and synchronization errors $\mathbf{e}_i(t)$ and $\boldsymbol{\varepsilon}_i(t)$ converge to zero, a cross-coupling error $\mathbf{e}_i^*(t)$ is defined to combine these two errors as the following equation:

$$\mathbf{e}_i^*(t) = \mathbf{e}_i(t) + \boldsymbol{\beta}\int_0^t \left(\boldsymbol{\varepsilon}_i(\omega) - \boldsymbol{\varepsilon}_{i-1}(\omega)\right) d\omega \tag{8}$$

Equation (7) can be rewritten as follows:

$$\mathbf{e}^*(t) = \mathbf{e}(t) + \boldsymbol{\beta}\int_0^t \boldsymbol{\rho}\boldsymbol{\varepsilon}(\omega) d\omega \tag{9}$$

where $\boldsymbol{\beta}$ is a positive gain matrix and ω is a time variable. Note that when $i=1$, $(i-1)=4$.

Substituting eq(6) into eq(8), we get:

$$\mathbf{e}^*(t) = \mathbf{e}(t) + \boldsymbol{\beta}\int_0^t \boldsymbol{\delta}\mathbf{e}(\omega) d\omega \tag{10}$$

where $\mathbf{e}^*(t), \mathbf{e}(t) \in \Re^{4\times 1}$, $\boldsymbol{\delta} = \mathbf{H}\boldsymbol{\rho} \in \Re^{4\times 4}$ are the defined matrixes.

Differentiating eq (9) with respect to time yields:

$$\dot{\mathbf{e}}^* = \dot{\mathbf{e}} + \boldsymbol{\beta}\boldsymbol{\delta}\mathbf{e} \tag{11}$$

Remark 1: Because $\boldsymbol{\beta}$ and $\boldsymbol{\delta}$ are selected as a positive matrix, both tracking error, $\mathbf{e}$, and syschronous error, $\boldsymbol{\varepsilon}$, will simultaneously obtain zero when the cross-coupling error, $\mathbf{e}^*$, is zero.

4. Control design

4.1. PID controller

PID is a controller, with a simple structure and is widely used in industrial applications. There is no requirement for a detailed mathematical model of the system for the PID controller design, so it is easy to apply in most real systems. For a 4-DOF parallel robot model, the PID control law takes the following form:

$$\boldsymbol{\tau} = \mathbf{K}_P\mathbf{e}(t) + \mathbf{K}_I\int_0^t \mathbf{e}(t)dt + \mathbf{K}_D\dot{\mathbf{e}}(t) \tag{12}$$

where $(\mathbf{K}_P, \mathbf{K}_I, \mathbf{K}_D) \in \Re^{4\times 4}$ are positive definite diagonal matrices of proportional, integral, and derivative respectively. $\mathbf{e}(t)$ is tracking error of active joints and $\dot{\mathbf{e}}(t) \in \Re^{4\times 1}$ is velocity error. Obviously, the PID control only takes into account controlling each of the active joints; hence, PID control is non-synchronous.

4.2. SPID controller

To solve the synchronization problem of parallel robots. A proposed synchronous controller combines a synchronous control algorithm and a conventional PID controller. The difference between a synchronous controller and traditional controllers is the response of synchronization error or the motion information of itself and of other joints. The motion coordination between the joints is considered, and the tracking ability of the end-effector is also improved. The structure of the SPID controller is exhibited in Figure 4.

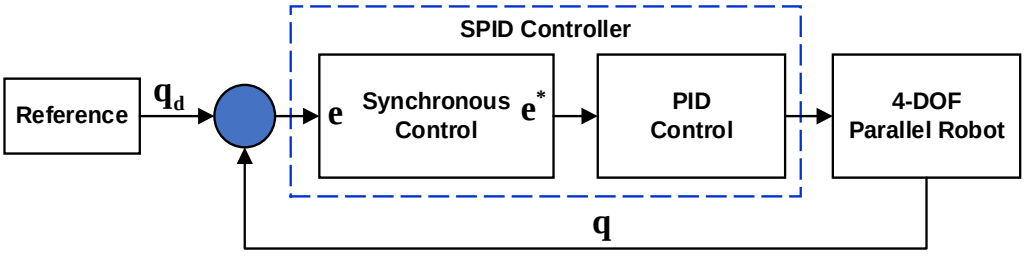

Figure 4 *The structure of the SPID controller*

The control law of the SPID is given as follows:

$$\boldsymbol{\tau} = \mathbf{K_p}\mathbf{e}^*(t) + \mathbf{K_I}\int_0^t \mathbf{e}^*(t)dt + \mathbf{K_D}\dot{\mathbf{e}}^*(t) \tag{13}$$

where $\mathbf{e}^*(t)$ is the cross-coupling error vector, $\dot{\mathbf{e}}^*(t)$ is the cross-coupling error velocity vector.

4.3. SMC controller

SMC is a nonlinear control approach that effects a nonlinear system's dynamics by applying a discontinuous control signal to cause the system to slide along its sliding surface. With the complex closed-chain structure, many singularity configurations, and geometric constraints, it is necessary to apply the SMC to the system. In order to improve the responsiveness of the system and make it operate steadily when orther unreliable factors are working on it. To design the SMC controller, a sliding surface is chosen as follows:

$$\mathbf{s}_1 = \boldsymbol{\lambda}\mathbf{e} + \dot{\mathbf{e}} \tag{14}$$

where $\mathbf{e} = \mathbf{q} - \mathbf{q_d}$, $\mathbf{e} \in \Re^{4\times1}$ is the position error vector, $\dot{\mathbf{e}} = \dot{\mathbf{q}} - \dot{\mathbf{q}}_\mathbf{d}$, $\dot{\mathbf{e}} \in \Re^{4\times1}$ is the velocity error vector, $\mathbf{q} \in \Re^{4\times1}$ is the response signal vector of the joint, $\mathbf{q_d} \in \Re^{4\times1}$ is the set signal vector of the joint, $\boldsymbol{\lambda} \in \Re^{4\times4}$ is a positive definite diagonal matrix, $\mathbf{s}_1 \in \Re^{4\times1}$ is the sliding surface variable vector.

The derivative of the equation (14) is:

$$\dot{\mathbf{s}}_1 = \boldsymbol{\lambda}\dot{\mathbf{e}} + \ddot{\mathbf{q}} - \ddot{\mathbf{q}}_\mathbf{d} \tag{15}$$

By substituting (5) into (15), the result is written as:

$$\dot{\mathbf{s}}_1 = \boldsymbol{\lambda}\dot{\mathbf{e}} - \ddot{\mathbf{q}}_\mathbf{d} + \mathbf{u} - \mathbf{d}(\mathrm{t}) \tag{16}$$

Sliding control law consists of two components: equilibrium and stability:

$$\mathbf{u} = \mathbf{u_{eq}} + \mathbf{u_r} \tag{17}$$

From (16), the equilibrium component, $\mathbf{u_{eq}} \in \Re^{4x1}$, is chosen when $\dot{\mathbf{s}}_1 = -\mathbf{k}\mathbf{s}_1$ and $\mathbf{d}(\mathrm{t}) = 0$.

$$\mathbf{u_{eq}} = -\boldsymbol{\lambda}\dot{\mathbf{e}} + \ddot{\mathbf{q}}_\mathbf{d} - \mathbf{k}\mathbf{s}_1 \tag{18}$$

where $\mathbf{K} \in \Re^{4x4}$ is a positive definite diagonal matrix and $\mathbf{u_r} \in \Re^{4x1}$ is the sustainable component calculated as follows:

$$\mathbf{u_r} = -\boldsymbol{\eta}\mathrm{sign}(\mathbf{s}_1) \tag{19}$$

where $\boldsymbol{\eta} \geq \| \mathbf{d}(\mathrm{t}) \|_\infty$, $\boldsymbol{\eta} \in \Re^{4\times4}$ is a positive definite diagonal matrix.

From (17), (18), and (19) the control law is deduced:

$$\mathbf{u} = -\boldsymbol{\lambda}\dot{\mathbf{e}} + \ddot{\mathbf{q}}_\mathbf{d} - \mathbf{k}\mathbf{s}_1 - \boldsymbol{\eta}\mathrm{sign}(\mathbf{s}_1) \tag{20}$$

Substituting equation (20) into (16), the equation is written as:

$$\dot{\mathbf{s}}_1 + \mathbf{k}\mathbf{s}_1 + \boldsymbol{\eta}sign(\mathbf{s}_1) + \mathbf{d}(\mathbf{t}) = 0 \tag{21}$$

The stability of the system is proved by choosing the following Lyapunov function:

$$V = \frac{1}{2}\mathbf{s}_1^{\mathrm{T}}\mathbf{s}_1 \tag{22}$$

The derivative of the equation (22) is presented as follows:

$$\dot{V} = \mathbf{s}_1^{\mathrm{T}}\dot{\mathbf{s}}_1 \tag{23}$$

Putting the (21) into (23) can yield:

$$\dot{V} = \mathbf{s}_1^{\mathrm{T}}\left(-\mathbf{k}\mathbf{s}_1 - \boldsymbol{\eta}\mathrm{sign}(\mathbf{s}_1) - \mathbf{d}(\mathrm{t})\right) \leq \mathbf{s}_1^{\mathrm{T}}\left(-\mathbf{k}\mathbf{s}_1 - \| \boldsymbol{\eta}\mathrm{sign}(\mathbf{s}_1) + \mathbf{d}(\mathrm{t}) \|_\infty\right) \leq -\mathbf{s}_1^{\mathrm{T}}\mathbf{k}\mathbf{s}_1 \tag{24}$$

Then, $\dot{V}$ is always negative because $\mathbf{k}$ is a positive definite matrix. So the system stable according to Lyapunov theory.

JTE HCMUTE
ISSN: 2615-9740
JOURNAL OF TECHNICAL EDUCATION SCIENCE
Ho Chi Minh City University of Technology and Education
Website: https://jte.edu.vn/
Email: jte@hcmute.edu.vn

4.4. SSMC controller

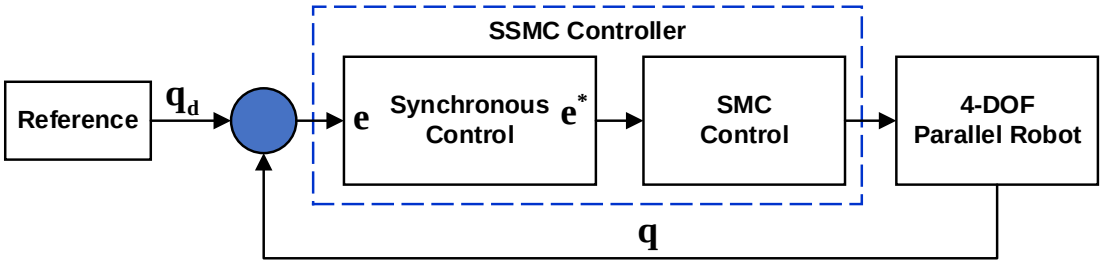

Figure 5. *The structure of the proposed control*

Similar to the PID controller, the SMC controller only performs individual control at each joint of the robot without considering the coordination of motion between the joints, or it can be said that the SMC controller is an asynchronous controller when applied to a system with a 4-DOF parallel robot. Therefore, in order to increase the tracking ability and solve the synchronization problem of the robot, an SSMC controller is proposed in Figure 5. Furthermore, the mode surface is designed based on the cross-coupling error to drive the system to achieve the goal of synchronization.

$$\mathbf{s}_2 = \boldsymbol{\lambda}\mathbf{e}^* + \dot{\mathbf{e}}^* \tag{25}$$

where $\mathbf{s}_2 \in \Re^{4\times1}$ is the sliding variable, $\boldsymbol{\lambda} \in \Re^{4\times4}$ is the positive definite diagonal matrices.

The differential sliding surface is calculated as:

$$\dot{\mathbf{s}}_2 = \boldsymbol{\lambda}\dot{\mathbf{e}}^* + \ddot{\mathbf{e}}^* \tag{26}$$

Remark 2: When $\mathbf{s}_2$ converges to 0 as $t \to \infty$, $\mathbf{e}^*$ converges to 0. When $\mathbf{e}^*(t) \to 0$ as $t \to \infty$ then $\mathbf{e}(t) \to 0$ and $\boldsymbol{\varepsilon}(t) \to 0$. When $\boldsymbol{\varepsilon}(t) \to 0$, the synchronization goal is achieved.

From (5) and (11), (26) can be rewritten as follows:

$$\begin{aligned}\dot{\mathbf{s}}_2 &= \boldsymbol{\lambda}\dot{\mathbf{e}}^* + \boldsymbol{\beta}\boldsymbol{\delta}\dot{\mathbf{e}} + \ddot{\mathbf{q}} - \ddot{\mathbf{q}}_\mathbf{d} \\ &= \boldsymbol{\lambda}\dot{\mathbf{e}}^* + \boldsymbol{\beta}\boldsymbol{\delta}\dot{\mathbf{e}} - \ddot{\mathbf{q}}_\mathbf{d} + \mathbf{u} - \mathbf{d}(t)\end{aligned} \tag{27}$$

SSMC controller has two components, equilibrium and robust, so the control law is described as:

$$\mathbf{u} = \mathbf{u}_{\mathbf{eq}} + \mathbf{u}_\mathbf{r} \tag{28}$$

From eq (27) equilibrium component $\mathbf{u}_{\mathbf{eq}} \in \Re^{4\times1}$ is chosen when $\dot{\mathbf{s}}_2 = -\mathbf{k}\mathbf{s}_2$ and $\mathbf{d}(t) = 0$.

$$\mathbf{u}_{\mathbf{eq}} = -\boldsymbol{\lambda}\dot{\mathbf{e}}^* - \boldsymbol{\beta}\boldsymbol{\delta}\dot{\mathbf{e}} + \ddot{\mathbf{q}}_\mathbf{d} - \mathbf{k}\mathbf{s}_2 \tag{29}$$

where $\mathbf{k} \in \Re^{4\times4}$ is the positive defined diagonal matrix.

A robust component $\mathbf{u}_\mathbf{r} \in \Re^{4\times1}$ is calculated as follows:

$$\mathbf{u}_\mathbf{r} = -\boldsymbol{\eta} sign(\mathbf{s}_2) \tag{30}$$

where $\boldsymbol{\eta} \geq \|\mathbf{d}(t)\|_\infty$, $\boldsymbol{\eta} \in \Re^{4\times4}$ is the positive define matrix.

From the (28), (29), and (30), we have the control law:

$$\mathbf{u} = -\boldsymbol{\lambda}\dot{\mathbf{e}}^* - \boldsymbol{\beta}\boldsymbol{\delta}\dot{\mathbf{e}} + \ddot{\mathbf{q}}_\mathbf{d} - \mathbf{k}\mathbf{s}_2 - \boldsymbol{\eta} sign(\mathbf{s}_2) \tag{31}$$

Substituting (31) into (27), we get:

$$\dot{\mathbf{s}}_2 + \mathbf{k}\mathbf{s}_2 + \boldsymbol{\eta}\,\mathrm{sign}(\mathbf{s}_2) + \mathbf{d}(\mathrm{t}) = 0 \tag{32}$$

To demonstrate the stability of the system, a Lyapunov function is chosen as follows:

$$V = \frac{1}{2}\mathbf{s}_2^\mathrm{T}\mathbf{s}_2 \tag{33}$$

The derivative of (33) with respect to time gives:

$$\dot{V} = \mathbf{s}_2^{\mathrm{T}}\dot{\mathbf{s}}_2 \tag{34}$$

Putting the equation (32) into (34) can yield:

$$\dot{V} = \mathbf{s}_2^{\mathrm{T}}\left(-\mathbf{k}\mathbf{s}_2 - \boldsymbol{\eta} sign(\mathbf{s}_2) - \mathbf{d}(t)\right) \le \mathbf{s}_2^{\mathrm{T}}\left(-\mathbf{k}\mathbf{s}_2 - \left\|\boldsymbol{\eta} sign(\mathbf{s}_2) + \mathbf{d}(t)\right\|_\infty\right) \le -\mathbf{s}_2^{\mathrm{T}}\mathbf{k}\mathbf{s}_2 \tag{35}$$

When $\mathbf{k}$ is selected as a positive definite matrix, $\dot{V}$ will be seminegative definite matrix. As mentioned in SMC, the sliding surface will asymptotically converge to zero in infinite time. From remark 2, whole controlled system is stable and both tracking and synchronous goals are achieved.

5. Results and Discussion

In this section, the experimental results of four control approaches are presented and evaluated to demonstrate the effect of the proposed algorithm. The circular trajectory is generated, as shown in Figure 6, and Table 1 displays the parameters of the controllers.

Table 1. *Parameters of the controllers*

Controllers	Values
PID	$\mathbf{K_p} = diag\left(\begin{bmatrix}40 & 40 & 36.5 & 36.5\end{bmatrix}\right)$; $\mathbf{K_I} = diag\left(\begin{bmatrix}0.5 & 0.5 & 0.001 & 0.001\end{bmatrix}\right)$; $\mathbf{K_D} = diag\left(\begin{bmatrix}0.2 & 0.2 & 0.25 & 0.25\end{bmatrix}\right)$.
SPID	$\mathbf{K_p} = diag\left(\begin{bmatrix}40 & 40 & 36.5 & 36.5\end{bmatrix}\right)$; $\mathbf{K_I} = diag\left(\begin{bmatrix}0.5 & 0.5 & 0.001 & 0.001\end{bmatrix}\right)$; $\mathbf{K_D} = diag\left(\begin{bmatrix}0.2 & 0.2 & 0.25 & 0.25\end{bmatrix}\right)$; $\boldsymbol{\beta} = diag\left(\begin{bmatrix}2 & 2 & 2 & 2\end{bmatrix}\right)$.
SMC	$\boldsymbol{\lambda} = \mathrm{diag}\left(\begin{bmatrix}270 & 270 & 250 & 240\end{bmatrix}\right)$; $\mathbf{k} = \mathrm{diag}\left(\begin{bmatrix}0.2 & 0.18 & 0.15 & 0.2\end{bmatrix}\right)$; $\boldsymbol{\eta} = \mathrm{diag}\left(\begin{bmatrix}0.025 & 0.025 & 0.025 & 0.025\end{bmatrix}\right)$.
SSMC	$\boldsymbol{\lambda} = \mathrm{diag}\left(\begin{bmatrix}270 & 270 & 250 & 240\end{bmatrix}\right)$; $\mathbf{k} = \mathrm{diag}\left(\begin{bmatrix}0.2 & 0.18 & 0.15 & 0.2\end{bmatrix}\right)$; $\boldsymbol{\eta} = \mathrm{diag}\left(\begin{bmatrix}0.025 & 0.025 & 0.025 & 0.025\end{bmatrix}\right)$; $\boldsymbol{\beta} = \mathrm{diag}\left(\begin{bmatrix}2 & 2 & 2 & 2\end{bmatrix}\right)$.

The circle orbit is given as follows:

$$\begin{cases} P_x = 100\cos(0.2\pi t) \\ P_y = 100\sin(0.2\pi t) \\ P_z = -500 \end{cases} \tag{36}$$

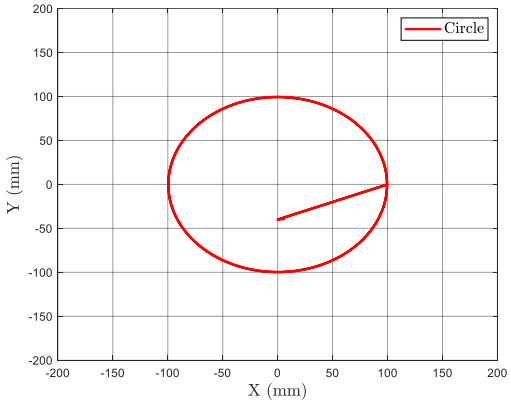

Figure 6. *The circle trajectory planning*

From eq (36) at each sampling time t, we get the position value of the end-effector. Then, the result of inverse kinematics is used with the input as position. We obtain the joint angle value, which is desired value of the $ith(i = 1,2,3,4)$ arm, as shown in Figure 7.

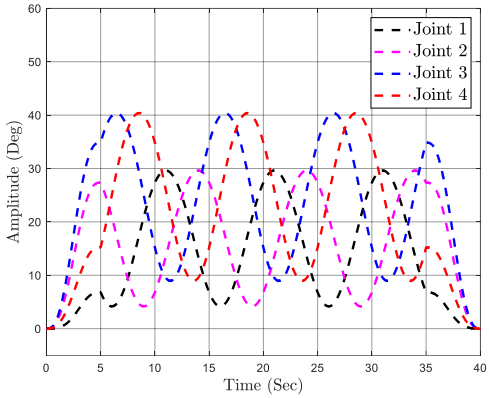

Figure 7. *The reference signals at the joints*

When alternately applying different controllers to the system to perform the preset trajectory tracking, we obtain the response signals at the joints of the robot and compare them with the reference signal in the following figure:

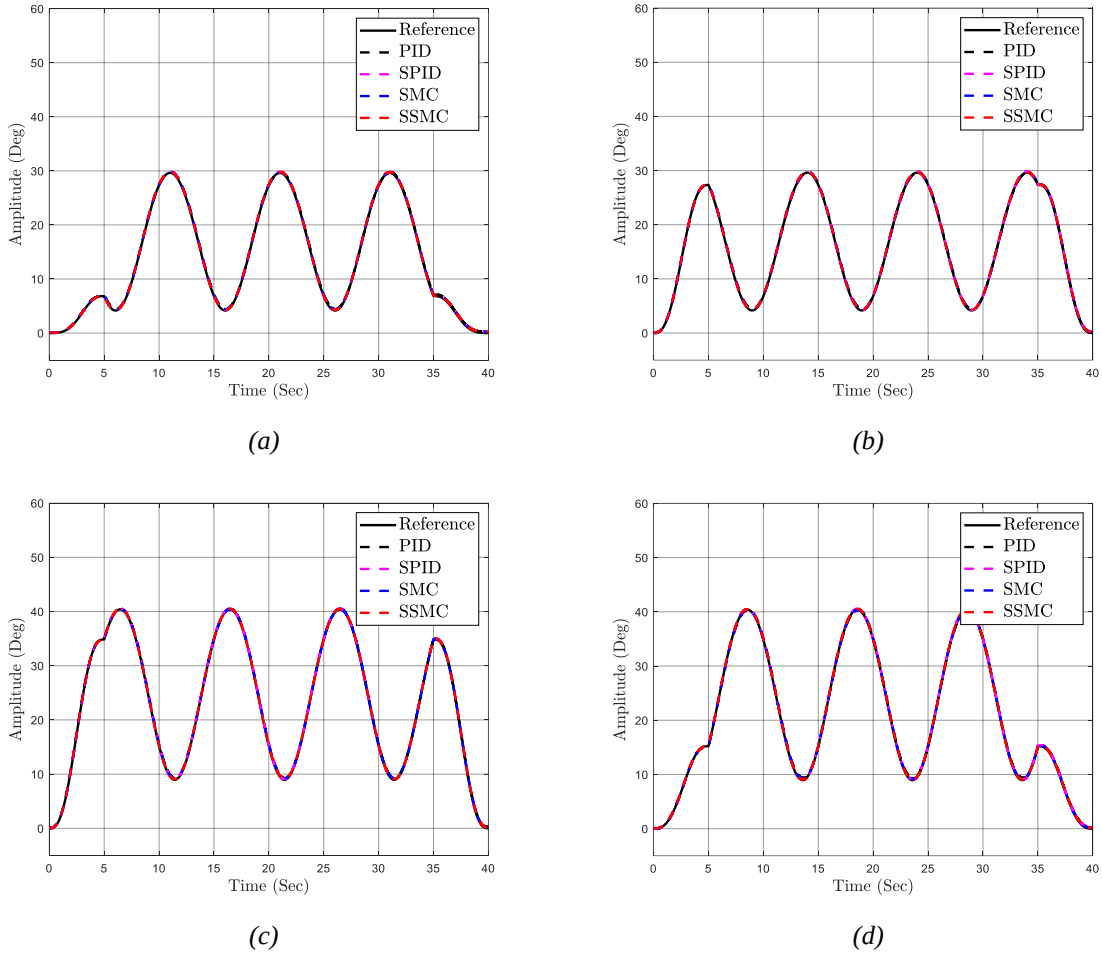

Figure 8. *Desired and response signals at the joints: (a) Joint 1; (b) Joint 2; (c) Joint 3; (d) Joint 4*

Figure 8 (a), (b), (c), (d) present the desired, and response at 4 joints of the robot in time corresponding to each controller with the trajectory described above. The graphs show the response signals of the joints tracking closely relative to the reference signal. It is difficult to realize the advanstages of the controllers in Figure 8. For readability, the tracking error are collected from the experimental process of the controllers and are plotted on the same graph according to time.

Figure 9 shows the tracking error of active joint 1, joint 2, joint 3, joint 4, respectively, when applying four controllers in the experiment – the black dot-line and blue dot-line signal tracking errors of the asynchronous PID and SMC, respectively. The pink dot-line and red dot-line are signal tracking errors of the synchronous SPID and SSMC, respectively. It is difficult to realize the improvement of the synchronous controllers in Figure 9. Then, some computations are implemented with the tracking errors accroding to the root means square error (RMSE) in Appendix. The results are in Table 2 demonstrated that the SPID and SSMC respectively give more accuracy than the PID and SMC. But they are not significantly.

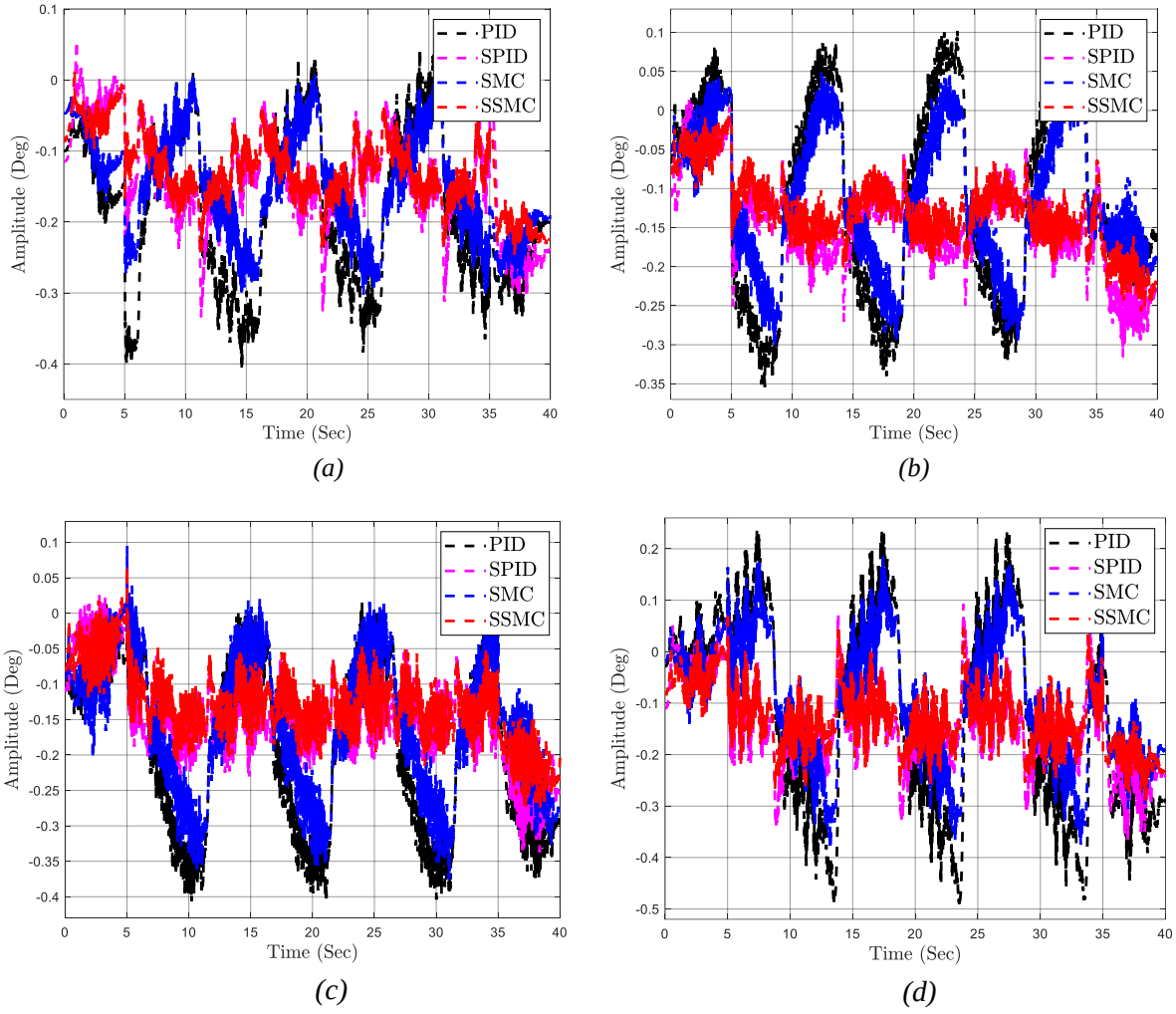

Figure 9. *Tracking errors of active joints: (a) Joint 1; (b) Joint 2;(c) Joint 3;(d) Joint 4*

Table 2. *Root mean square of the tracking errors*

Controllers	Joint 1	Joint 2	Joint 3	Joint 4
PID	0.2140	0.1683	0.2208	0.2298
SPID	0.1604	0.1560	0.1564	0.1659
SMC	0.1680	0.1651	0.1843	0.1684
SSMC	0.1388	0.1370	0.1386	0.1437

Next, to see the synchronization of the system as well as the deviation of two adjacent joints when there is no synchronization and when there is synchronization. Finally, the synchronization error of the system is shown in Figure 10**.**

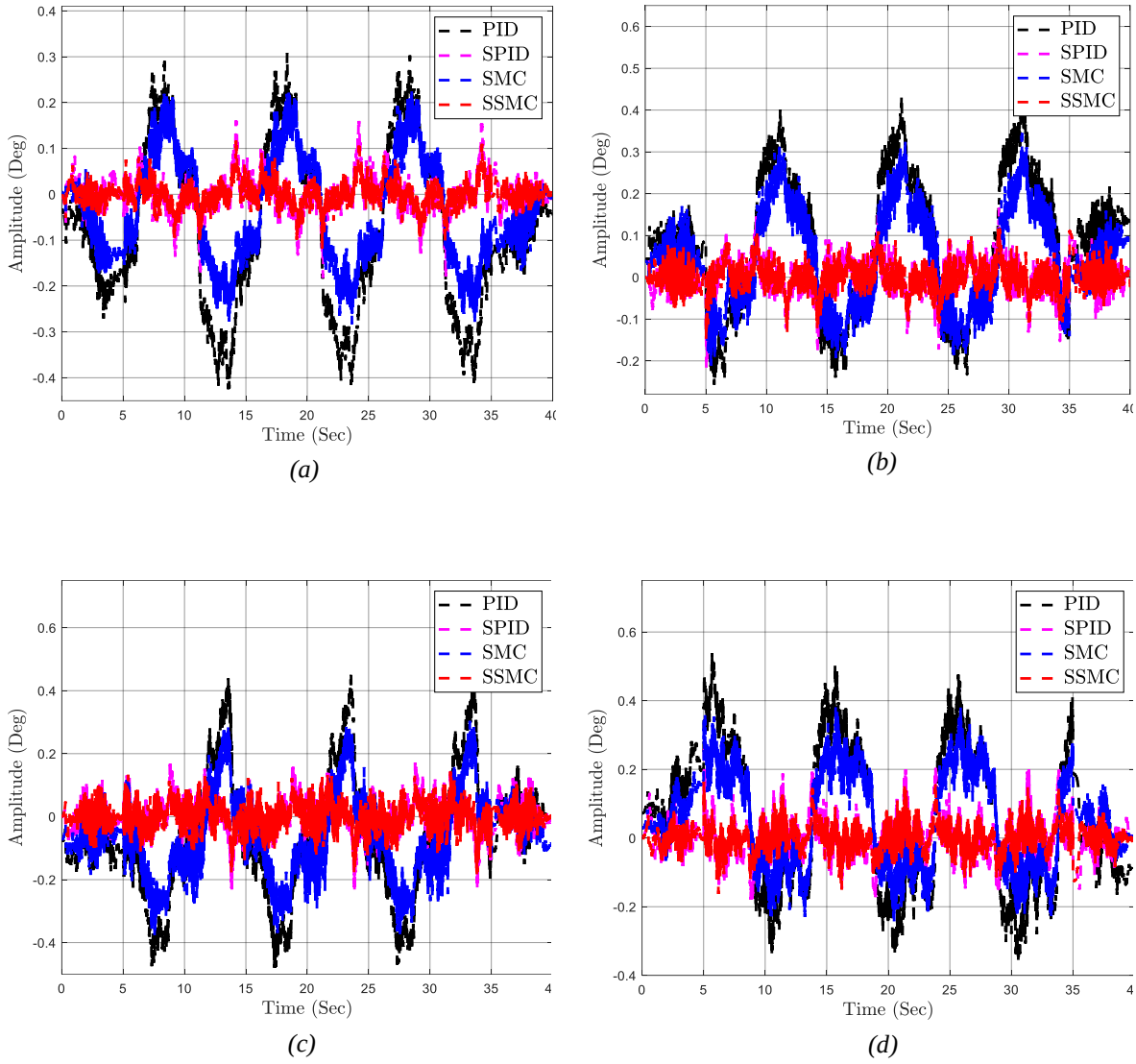

Figure 10. *Synchronization error between the active joints: (a) Joint 1&2; (b) Joint 2&3; (c) Joint 3&4; (d) Joint 4&1*

Figure 10 presents the synchronization error of Joint 1&2, Joint 2&3, Joint 3&4, and Joint 4&1, respectively. According to the figures, we can see that the synchronization error of synchronous controllers is smaller than that of conventional controllers, or the difference between two adjacent joints of synchronous controllers is significantly reduced. Therefore, the performance of the controllers is improved, especially the SSMC controller. Similar to the tracking error, the RMSE of the synchronization errors is also computed by (37). The results in Table 3 proved that the synchronous errors of the synchronous PID controller and SSMC are respectively better than the PID controller and the SMC.

Table 3. *Root mean square of the synchronization errors*

Controllers	Joint 1&2	Joint 2&3	Joint 3&4	Joint 4&1
PID	0.1915	0.1766	0.2	0.2188
SPID	0.0426	0.0428	0.0559	0.0586
SMC	0.1215	0.1243	0.1433	0.1488
SSMC	0.0280	0.0341	0.0440	0.0405

Based on the above analysis, the results demonstrate the synchronous controllers improved accuracy of not only tracking errors but also the synchronous errors. Additionally, the above results also demonstrate that for closed-loop systems, the system performance and end-effector tracking capability of the robot are significantly improved when the synchronization between the actuators is achieved.

6. Conclusion

In this paper, a SSMC controller is developed for a 4-DOF parallel robot model in practice. The proposed controller can provide good properties, such as resistance to external noise and uncertain dynamics of the SMC method, and the movement between joints is considered by the synchronization algorithm. A sliding surface has been designed based on the cross-coupling error. So, the suggested control receives the motion data of each joint and from its two adjacent joints. The design of the SSMC controller is based on this sliding surface. Then the synchronization goal of the system is achieved, and the simultaneous reduction of tracking and synchronization errors towards zero. In addition, the Lyapunov theory has been used to show that the system is stable. In order to verify the effectiveness of the proposed approach further, a 4-DOF parallel robot testbench was constructed, and the experimental results of the proposed control were compared to three other controllers.

Acknowledgments

This work belongs to the project grant No: B2022-SPK-03. funded by Ministry of Education and Training, and hosted by Ho Chi Minh City University of Technology and Education, Vietnam.

Appendix

To accurately evaluate the performance of each controller, the root means squared error (RMSE) method is used based on a set of data collected from the experimental process of the controllers. We have the formula of the RMSE method as follows:

$$RMSE = \sqrt{\frac{1}{n}\sum_{i=1}^{n}\left(s_i - o_i\right)^2} \tag{37}$$

where n is samples of modeling errors, s_i is the set value, o_i is the response value.

REFERENCES

[1] K. C. Dinh, N. S. Dao, H. D. Le, H. L. Le, T. D. T. Cam, and D. T. Tran, "Kinematics and Dynamics for a 4-DOF Parallel Robot," presented at the 2021 International Conference on System Science and Engineering (ICSSE), 2021.
[2] F. Pierrot, V. Nabat, O. Company, S. Krut, and P. Poignet, "Optimal Design of a 4-dof Parallel Manipulator," (in E), *IEEE Transactions on Robotics*, vol. 25, no. 2, pp. 213-224, 2009.
[3] C. Yang, Q. Huang, H. Jiang, O. O. Peter, J. Han, "PID control with gravity compensation for hydraulic 6-DOF parallel manipulator," (in E), *Mechanism and Machine Theory*, vol. 45, no. 4, pp. 666-677, 2011.
[4] A. J. Humaidi and A. I. Abdulkareem, "Design of Augmented Nonlinear PD Controller of Delta/Par4-Like Robot," *Journal of Control Science and Engineering*, vol. 2019, pp. 1-11, 2019.
[5] Y. X. Su, B. Y. Duan, and C. H. Zheng, "Nonlinear PID control of a six-DOF parallel manipulator," *IEE Proceedings - Control Theory and Applications*, vol. 151, no. 1, pp. 95-102, 2004.
[6] Z. Yang, J. Wu, J. Mei, J. Gao, and T. Huang, "Mechatronic Model Based Computed Torque Control of a Parallel Manipulator," (in E), *International Journal of Advanced Robotic Systems*, vol. 5, no. 1, 2008, doi: https://doi.org/10.5772/5650.
[7] W. Shang and S. Cong, "Nonlinear computed torque control for a high-speed planar parallel manipulator," *Mechatronics*, vol. 19, no. 6, pp. 987-992, 2009.
[8] W. W. Shang, S. Cong, and Y. Ge, "Adaptive computed torque control for a parallel manipulator with redundant actuation," *Robotica*, vol. 30, no. 3, pp. 457-466, 2011.
[9] Y. Koren, "Cross-Coupled Biaxial Computer Control for Manufacturing Systems," *Journal of Dynamic Systems, Measurement, and Control*, vol. 102, no. 4, p. 265, 1980.
[10] Y. X. Su, D. Sun, L. Ren, X. Wang, and J. K. Mills, "Nonlinear PD Synchronized Control for Parallel Manipulators," *International Conference on Robotics and Automation*, Barcelona, Spain, 2005, pp. 1374-1379, doi: 10.1109/ROBOT.2005.1570307.
[11] T. T. C. Duong, C. C. Nguyen, and T. D. Tran, "Synchronization Sliding Mode Control of Closed-Kinematic Chain Robot Manipulators with Time-Delay Estimation," *Appl. Sci.*, vol. 12, no. 11, p. 5527. 2022.
[12] T. T. C. Duong, T. D. Thien, N. T. Tri, and D. V. Nghi, "Synchronization Sliding Mode Control with Time-Delay Estimation for a 2 DOF Closed-Kinematic Chain Robot Manipulator," presented at the 2021 International Conference on System Science and Engineering (ICSSE), Ho Chi Minh City, Vietnam, 2021, pp. 38-43, doi: 10.1109/ICSSE52999.2021.9538491.
[13] Y. Pi, X. Wang, X. Gu, "Synchronous tracking control of 6-DOF hydraulic parallel manipulator using cascade control method," *J. Cent. South Univ. Technol.*, vol. 18, pp. 1554–1562, 2011.
[14] J. P. Merlet, *Parallel Robots*, second ed. Springer, 2006.

Tran Duc Thien received the B.S and M.S. degrees in the Department of Electrical Engineering, Ho Chi Minh City University of Technology, Vietnam, in 2010, 2013, and the Ph.D. degree from University of Ulsan in 2020, respectively.
He works as a lecturer with the Department of Automatic Control, Ho Chi Minh City University of Technology and Education (HCMUTE), Vietnam. His research interests include robotics, variable stiffness system, fluid power control, disturbance observer, nonlinear control, adaptive control, and intelligent technique. Email: thientd@hcmute.edu.vn

Nguyen Thanh Nha received the diploma of engineer majoring in control engineering and automation from the Faculty For High-Quality Training, Ho Chi Minh City University of Technology and Education, Vietnam, in 2023.
He works as a Robotics and Intelligent Control Lab member in the Department of Automatic Control, Ho Chi Minh University of Technology and Education, Vietnam.
His research interests include robotics, parallel robot, nonlinear control, and intelligent control. Email: ntnha0639@gmail.com

Nguyen Minh Tam received the B.E degree in Electrification and Electrical Power Supply from Ho Chi Minh City University of Technical Education, Vietnam, the Masters degree in Electrical Engineering from Ho Chi Minh City University of Technology, Vietnam and the Ph.D. degree in Engineering Science from the University of Technology, Sydney in 1995, 2003 and 2010 respectively. He is the current lecturer at the Control Engineering and Automation Department. He is the current Dean of Faculty of Electrical and Electronic Engineering at Ho Chi Minh City University of Technology and Education, Vietnam. His research interests include system modelling, intelligent and robust control, and soft-computing. Email: tamnm@hcmute.edu.vn

Ngo Van Thuyen received the B.E degree in electrical engineering from Ho Chi Minh City University of Technology and Education, Vietnam in 1999, the M.E degree in electrical engineering Ho Chi Minh City University of Technology, Vietnam in 2003, and the PhD degree in engineering from University of Technology Sydney, Australia in 2008.
He is currently an associate professor at the Department of Automatic Control, Ho Chi Minh City University of Technology and Education (HCMUTE), Vietnam. His research interests include mobile robotics, nonlinear control, adaptive control, and intelligent technique. Email: thuyennv@hcmute.edu.vn

Le Hoang Lam received the B.S. degree and M.S degree in in Power Engineering from Ho Chi Minh City University Of Technology, VietNam in 2006 and 2008. He is currently a lecturer at the Faculty of Electrical and Electronic Engineering, Ho Chi Minh City University of Technology and Education. His research interest includes the precise position synchronous control for multi-axis servo systems. Email: lamlh@hcmute.edu.vn